Naval Research Laboratory
Washington, DC 20375-5320

NRL/5509/MR—2023/3

Optimized Reduced Spectrum Models of Diffuse Reflectance for NIR-SWIR Absorbing-Dye Formulations

RACHEL VIGER, PA

SCOTT A. RAMSEY

TROY MAYO

Signature Technology Office
Systems Directorate Division

SAMUEL G LAMBRAKOS

Mission Development Branch
Space Systems Development Division

November 9, 2023

REPORT DOCUMENTATION PAGE

Form Approved
OMB No. 0704-0188

1. REPORT DATE *(DD-MM-YYYY)*	**2. REPORT TYPE**	**3. DATES COVERED** *(From - To)*
09-11-2023	NRL Memorandum Report	

4. TITLE AND SUBTITLE

Optimized Reduced Spectrum Models of Diffuse Reflectance for NIR-SWIR Absorbing-Dye Formulations

5a. CONTRACT NUMBER

5b. GRANT NUMBER

5c. PROGRAM ELEMENT NUMBER

6. AUTHOR(S)

Rachel Viger, PA, Scott A. Ramsey, Troy Mayo, and Samuel G. Lambrakos

5d. PROJECT NUMBER

5e. TASK NUMBER

5f. WORK UNIT NUMBER
2401

7. PERFORMING ORGANIZATION NAME(S) AND ADDRESS(ES)

Naval Research Laboratory
4555 Overlook Avenue, SW
Washington, DC 20375-5320

8. PERFORMING ORGANIZATION REPORT NUMBER

NRL/5009/MR--2023/3

9. SPONSORING / MONITORING AGENCY NAME(S) AND ADDRESS(ES)

Naval Research Laboratory
4555 Overlook Avenue, SW
Washington, DC 20375-5320

10. SPONSOR / MONITOR'S ACRONYM(S)

NRL Edison Program

11. SPONSOR / MONITOR'S REPORT NUMBER(S)

12. DISTRIBUTION / AVAILABILITY STATEMENT

DISTRIBUTION STATEMENT A: Approved for public release; distribution is unlimited.

13. SUPPLEMENTARY NOTES

14. ABSTRACT

This study describes a measurement-optimized parametric model of diffuse reflectance, based on the reduction of absorption spectra for Near Infrared (NIR) and Short-Wave Infrared (SWIR) absorbing dyes on substrates using critical feature isolation and projection. The critical features are identified through a structural analysis of the peaks, troughs, and points of inflection within the Kubelka-Munk absorption spectra, which is calculated from diffuse reflectance measurements. These critical features are then parameterized and projected into a reduced feature subspace using Lorentzian decompositions to effectively capture the fundamental characteristics of the absorbing dyes, while removing processing and measurement noise. A Kramers-Kronig analysis then characterizes the dielectric responses and provides an estimation of the reduced spectra reflectance. The model parameters for the analytical reduction are further refined using a nonlinear multivariable optimization function between the analytically predicted reflectance and the measured reflectance. This results in an enhanced measurement-optimized model that is capable of incorporating measurement and processing artifacts to improve application-specific reflectance predictions. Furthermore, the reduced, enhanced functions establish a parametric dataspace that can support the mapping of functions between individual NIR-SWIR absorbing dye components and the diffuse reflectance predictions for new mixture and substrate combinations.

15. SUBJECT TERMS

Absorption spectra
Parametric modeling
Feature projection

16. SECURITY CLASSIFICATION OF:			**17. LIMITATION OF ABSTRACT**	**18. NUMBER OF PAGES**	**19a. NAME OF RESPONSIBLE PERSON**
a. REPORT	**b. ABSTRACT**	**c. THIS PAGE**			Rachel Viger
U	U	U	U	25	**19b. TELEPHONE NUMBER** *(include area code)* (202) 279-5249

Standard Form 298 (Rev. 8-98)
Prescribed by ANSI Std. Z39.18

This page intentionally left blank.

Table of Contents

This page intentionally left blank.

1. Introduction

This study describes a parametric model of diffuse reflectance from Near Infrared (NIR) and Short-Wave Infrared (SWIR) absorbing dyes on cotton-fabric substrates [1]. The parametric models provide representation of dielectric-response characteristics of the dyes and information on the sensitivity of their interactions with substrates. The parametric model is based reduction of absorption spectra by means of critical feature isolation and projection. The critical features are identified through structural analysis of the peaks, troughs, and points of inflection in the calculated Kubelka-Munk absorption spectra from diffuse reflectance measurement [2-5]. These features are then parameterized and projected into a reduced feature subspace to effectively capture the fundamental characteristics of the absorbing dyes, while still maintaining the essence of the critical features. The critical feature parameterization and projection supports the construction of the parametric model which is capable of simulating reflectance from coated substrates, for various dyes, substrates, and mixtures. The IR-absorbing dyes considered in this study are characterized by robust spectral features, whose inverse spectral analysis demonstrate the concept, as emphasized by reference [6], of applying Kramers-Kronig analysis to diffuse reflectance [7-9], which has significant practical value with respect to reduced effort for sample preparation (for spectroscopic analysis). Construction of reduced feature spaces for spectrum characterization is based on concepts from principle-component analysis (PCA) [10]. Sample preparation for spectroscopic measurements and the IR-absorbing dyes considered in this study are described in reference [11] and references [12,13], respectively. This study continues examination of inverse analysis and parametric modeling of NIR and SWIR absorbing dyes on cotton-fabric substrates [14, 15, 16]

The reduced subspace models produce an undressed spectra that preserves the critical dye characteristics, while removing undesired spectral noise and complexity. This allows for a simplified analytical expression for each NIR-SWIR absorbing dye. Extending this analysis to multiple dyes provides a database of analytical representations for the individual dyes and their significant features. These undressed functions also provide a noise-free initial representation of the dyes that support the construction of the measurement-enhanced models. These models are constructed using a constrained multivariable optimization to account for measurement artifacts within the diffuse reflectance. This establishes an enhanced measurement-based version of the modeling space that can improve application-specific reflectance predictions. This modeling subspace can then support the construction of effective-medium models for mixtures and deposit-on-substrate micro or meso structures.

Effective medium models work by defining a weighted relationship between the constituent dyes and substrates that make up a composite NIR-SWIR absorbing mixture. Using the reduced, enhanced analytical representations of the individual dye constituents allows these effective medium models to analytically predict the macroscopic properties of new composite mixtures. Since these models are created using a parametric subspace, this allows for additional algorithmic approaches for identifying the spectral mappings between the individual reduced spectra and the new dye mixture combinations. Future efforts will explore the spectral prediction accuracy of such models.

Manuscript approved October 30, 2023.

2. Undressed Parametric Model of Diffuse Reflectance Spectra

The Kramers-Kronig analysis provides an estimation of dielectric responses using diffuse reflectance from materials on substrates and their absorption functions obtained using inverse-analysis. The initial methodology for calculating the complex dielectric response function of the undressed spectra follows a similar procedure to that developed in Ref. [16]. This reference describes the previous research focused on estimating the dielectric response functions for NIR-SWIR absorbing dyes. This effort now extends this analysis and uses reduced analytical representations of the calculated absorption to create optimized models of the diffuse reflectance, capable supporting new dye mixture predictions.

For this analysis, normalized extinction functions $\langle \alpha_N(\lambda) \rangle$, dependent on wavelength λ, are determined by inverse spectral analysis of diffuse-reflectance spectra using the Kubelka-Munk model, i.e.,

$$\langle \alpha_N(\lambda) \rangle = \frac{f_{KM}(\lambda)}{\max[f_{KM}(\lambda)]} \qquad (Eq.\,1)$$

and

$$f_{KM}(\lambda) = \frac{\left(1 - R_n(\lambda)\right)^2}{2R_n(\lambda)}. \qquad (Eq.\,2)$$

where R_n is the normalized reflectance relative to background, e.g., substrate, and f_{KM} is the Kubelka-Munk absorption estimate. Before proceeding, it should be noted that the inversion procedure defined by Eqs. (1) and (2) has a specific sensitivity property with respect to NIR-SWIR absorbing dyes, and accordingly, is essentially equivalent to other inversion procedures, applied to different types of spectroscopic measurements. This sensitivity property is discussed below.

Next, an imaginary index of refraction, $k_N(\lambda)$, scaled according to the normalized extinction functions $\langle \alpha_N(\lambda) \rangle$, is calculated by

$$\langle k_N(\lambda) \rangle = \frac{\langle \alpha_N(\lambda) \rangle \lambda}{4\pi}, \qquad (Eq\ 3)$$

and a real-refractive-index change, $\Delta n_N(\lambda)$, consistently scaled, is calculated by the Kramers-Kronig relation

$$\langle \Delta n_N(\lambda) \rangle = \frac{2\lambda^2}{\pi} P \int_0^\infty \frac{\langle k_N(z) \rangle dz}{z(\lambda^2 - z^2)}. \qquad (Eq\ 4)$$

Note that a multiplicative factor approximates the dependence on scatterer density, and that the Kubelka-Munk function in Eq. (2) is correlated with the absorbance function. Further, we assume that the wavelength integration range of Eq. (4) is incomplete, but of sufficient expanse for estimation of the real-refractive-index change $\langle \Delta n_N(\lambda) \rangle$. Sensitivity with respect to this incompleteness can be quantified by extrapolation procedures at the limits of the measured spectral range.

Adopting the approximation of a scattering coefficient C_{scat} as being weakly dependent on wavelength, it follows that the normalized extinction function is dependent on the wavelength dependent absorption coefficient and a multiplicative factor used to approximate the dependence on scatterer density. The scaling parameter C_s represents this dependence on scatterer density, and the normalized absorption estimate, $\alpha_s(\lambda)$, is represented by:

$$\alpha_s(\lambda) = C_s\langle\alpha_N(\lambda)\rangle. \qquad (Eq\ 5)$$

Accordingly, the dependence of the complex index of refraction on scatterer density is

$$k_s(\lambda) = C_s\langle k_N(\lambda)\rangle \qquad (Eq\ 6)$$

and

$$n_s(\lambda) = 1 + C_s\langle\Delta n_N(\lambda)\rangle. \qquad (Eq\ 7)$$

Additional information on the Kramers-Kronig calculation and the scatterer density significance can be found in Ref. [16]. Numerical integration of Eq. (4) uses methods described in references [7-9]. The spectral-reduction procedure entails the decomposition of $\langle\alpha_N(\lambda)\rangle$ in terms of reduced basis-function expansions, consisting of Lorentzian functions. Thus integration defined by Eq. (4) is performed analytically, by Hilbert transformation of analytic functions. Accordingly, letting

$$\langle\alpha_N(\lambda)\rangle = \lambda \sum_{k=1}^{N_k} \left(\frac{A_k}{\lambda_k}\right) \frac{(\gamma_k/2)^2}{(\lambda-\lambda_k)^2 + (\gamma_k/2)^2} \quad , \qquad (Eq.8)$$

it follows that

$$\langle k_N(\lambda)\rangle = \frac{\lambda^2}{4\pi} \sum_{k=1}^{N_k} \left(\frac{A_k}{\lambda_k}\right) \frac{(\gamma_k/2)^2}{(\lambda-\lambda_k)^2 + (\gamma_k/2)^2} \qquad (Eq.9)$$

and

$$\langle\Delta n_N(\lambda)\rangle = \frac{\lambda^2}{4\pi} \sum_{k=1}^{N_k} \left(\frac{A_k}{\lambda_k}\right) \frac{(\gamma_k/2)(\lambda-\lambda_k)}{(\lambda-\lambda_k)^2 + (\gamma_k/2)^2}\,. \qquad (Eq.10)$$

A parametric model of reflectance is given by:

$$R_M(\lambda) = R_B(\lambda)[1 - R_s(\lambda)] \qquad (Eq.11)$$

where

$$R_s(\lambda) = \frac{[n_s(\lambda)-1]^2 + [k_s(\lambda)]^2}{[n_s(\lambda)+1]^2 + [k_s(\lambda)]^2} \qquad (Eq.12)$$

and $R_B(\lambda)$ is the substrate reflectance. An algorithm and case study analyses for the decomposition of $\langle\alpha_N(\lambda)\rangle$ in terms of reduced basis-function expansions, consisting of Lorentzian functions, is

given in reference [15]. This decomposition can be achieved because key features of IR spectra, e.g., those of IR absorbing dyes, including their absorption peaks and troughs, can be characterized within a dimensionally reduced space using concepts from principle-component analysis (PCA) [10]. Accordingly, full spectral data can be projected into a smaller subspace of spectral components, while still maintaining the essence of the critical features, such as peak wavelengths, peak heights, and inflection points.

With respect to the inverse spectral analysis, the parametric model defined by Eqs. (11) and (12) is not considered a unique representation, but rather part of a concept model space. The choice of a particular parametric model within a model space is motivated by the property obtained by the inverse analysis (e.g. complex indices of refraction) and the system characteristics to be simulated (e.g. scatterer mixing and segmentation on substrate), as well as the convenience of the model formulation for its combination with other models. The parametric model in Eqs. (11) and (12) has been formulated for combination with established effective-medium models and machine learning optimization methods, which themselves may be characterized as part of a model space.

3. Measurement-Optimized Parametric Model of Diffuse Reflectance Spectra

The undressed parametric models from Section 2 can be further modified to capture the spectral artifacts that emerge through the measurement process and instrumentation. This step incorporates a multi-variable optimization that adjusts the reduced spectral parameters, such that the modeled reflectance, calculated through Eq. (12), more accurately fits the measured diffuse reflectance. The function variables considered include the critical feature peak wavelengths, peak heights, peak widths, and the scattering density, C_s. The number of critical features is also adjusted such that the features provide sufficient spectral parameters, while still minimizing the model complexity.

The optimization function calculates the mean squared error between the measured diffused reflectance and the model calculated reflectance using the reduced spectrum parameters, as shown in Eq. 13, where $\overline{w}$ represents an array of the peak wavelength locations, $\bar{h}$ represents an array of the peak heights, and $\overline{w}$ represents an array of the peak full-widths at half height.

$$\min MSE = \min f(x) = \min\ f(\overline{w}, \bar{h}, \overline{w}, C_s) \qquad (Eq.13)$$

The mean squared error is calculated by the difference between the normalized reflectance relative to background, $R_n(\lambda)$, and the calculated reflectance through Eq. (12), $R_s(\lambda)$, as shown in Eq. (14).

$$MSE = \frac{1}{N}\sum_{\lambda=1}^{N}\left(R_n(\lambda) - R_s(\lambda)\right)^2 \qquad (Eq.14)$$

The reduced spectrum input parameters included the peak wavelengths, peak heights, peak full-width at half-height, and the scatter density. The optimization constraints for these parameters are shown in Table 1. The initial values for these parameters a provided through the undressed reduced spectra. For the critical features added beyond the undressed spectrum features, the parameters

were initialized such that the peak wavelengths evenly spanned the dyes absorption zone, and started with peak heights of 0.2 and peak full width half means of 40 nm.

Table 1: Multivariable Optimization Constraints

Step	Minimum	Maximum
Peak Wavelength	0 nm	2500 nm
Peak Height	0	1 (normalized)
Peak Full-Width at Half Height	0 nm	1000 nm
Scatter Density C_s	0	10

The iterative optimization follows a gradient-based descent algorithm that searches for a local minimum within the mean squared error. The parameters are finalized once the optimization tolerance is reached. These measurement-optimized reduced spectra parameters represent the critical feature reduction that can more accurately deconstruct the measurement spectrum, and in-turn support more accurate measurement-dependent predictions for new dye mixtures and substrates. The next section provides an example case for calculating and comparing the undressed reduced spectra and the measurement-optimized reduced spectra.

4. Example of Modeling Procedure

The dyes chosen for this analysis have maximum-absorption wavelengths in either the NIR or SWIR bands, with appreciable spectral features extending into the visible spectrum. Reference [11] describes the procedures used for dye and dyed-fabric sample preparation, and reflectance-spectrum measurements of dyed fabric samples. Reference [16] describes the spectrometer specifications the measurement process for the diffuse reflectance. For this study, these dyes are designated according to their maximum absorption wavelengths, using the designation "KM-Maximum-Absorption-Wavelength," similar to references [12,13], where the chemical formulae for these dyes are given. For each of these results, the absorption spectra was calculated from diffuse reflectance measurements using the normalized Kubelka-Munk inverse analysis method.

The initial critical feature isolation and projection for dye KM-720 is shown in Figure 1. The undressed subspace projection consists of four peaks as defined in Table 2. The undressed parameters are selected to optimally match the full spectral features. This significant reduction in the absorption spectra still sufficiently captures the dye's defining absorption characteristics.

KM-720

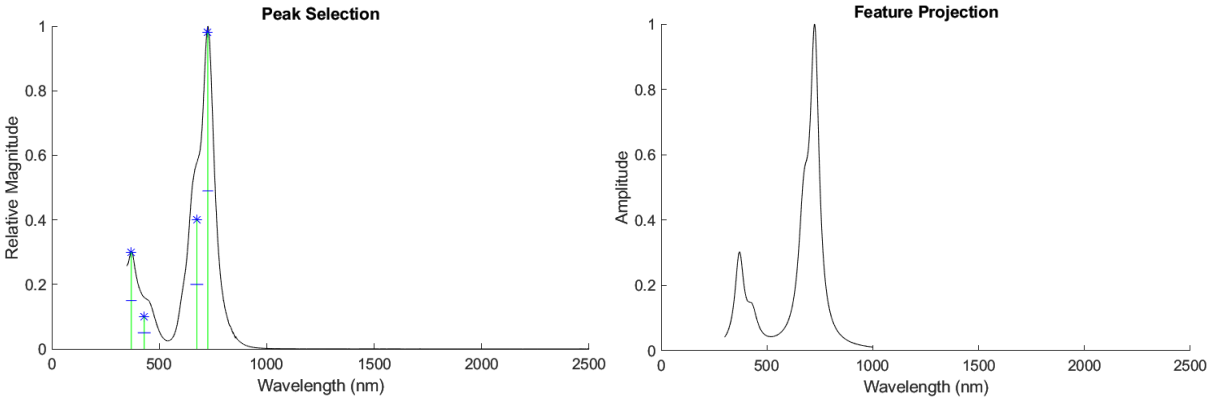

Figure 1: KM-720 absorption spectra and peak characterization, and comparison between the original Kubelka-Munk absorption spectra and the subspace feature projection.

Table 2: KM-720 Undressed Critical Peak Parameters

Wavelength	Peak Amplitude	Full-Width Half-Height
370	0.30	50
430	0.10	60
675	0.40	60
726	0.98	50

The complex indices of refraction for the reduced absorption subspaces were estimated and evaluated using Kramers-Kronig analysis Eqs. (9) and (10). Kramers-Kronig analysis establishes fundamental material properties that can support the characterization of the dielectric response functions. The intermediate index of refraction properties, $\Delta n_N(\lambda)$ and $k_N(\lambda)$, are of particular interest, as they can be scaled – based on the scatterer density – to effectively estimate these dielectric response functions. The Kramers-Kronig results from the undressed reduced subspace absorption were compared to the complex index of refraction for the full dataset with extrapolation, termination, and smoothing corrections, as calculated in reference [14]. The result of this comparison for KM-720 is shown in Figure 2.

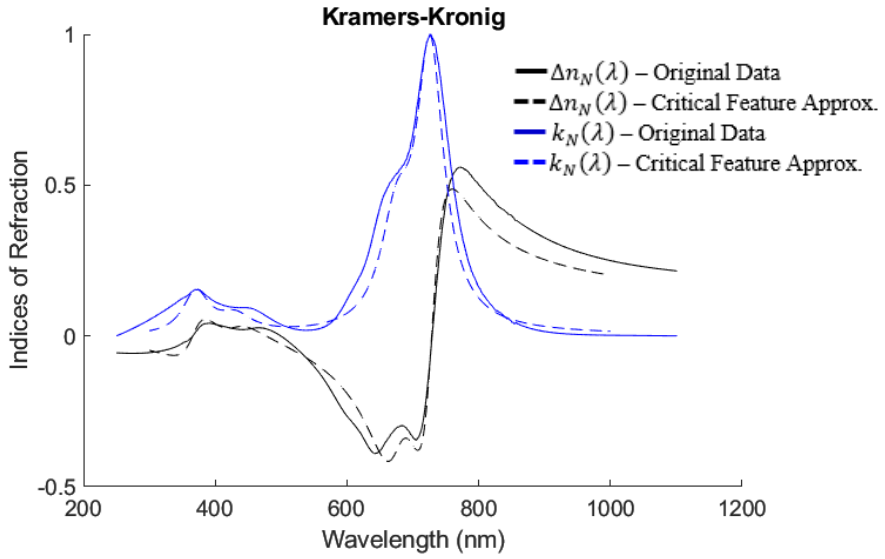

Figure 2: KM-720 Kramers-Kronig indices of refraction, comparing the results from the full extrapolated and smoothed KM dataset with the results from the critical feature approximation.

Using the scalable indices of refraction components, and the undressed spectra, a model for the diffuse reflectance was calculated using Eqs. (11) and (12). A comparison between the originally measured diffuse reflectance and the undressed model results is shown in Figure 3. The locations of the critical peaks align closely; however, there are significant differences between the trough and peak widths, as expected due to broadening effects. Therefore, the undressed reflectance model is limited in its ability to accurately capture the measurement and application artifacts. Therefore, a measurement-optimization is performed on the reduced spectra parameters to better align the calculated reflectance with the measured diffuse reflectance.

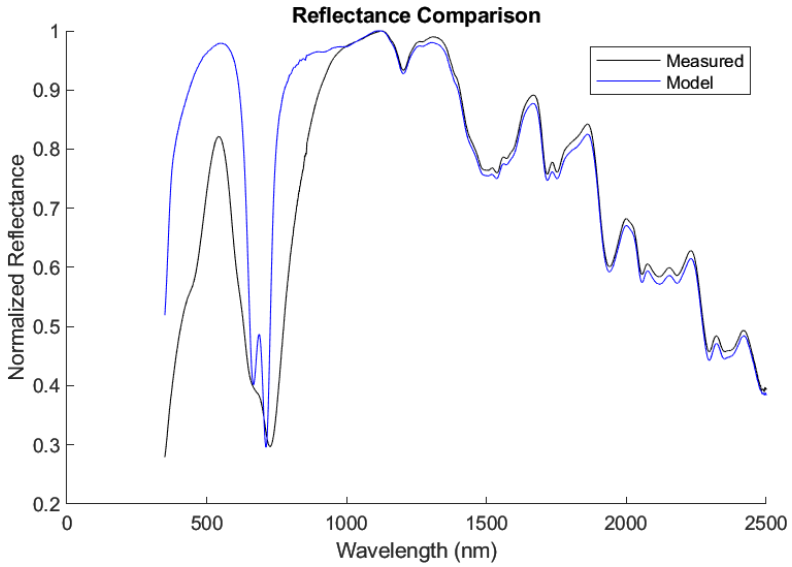

Figure 3: Comparison of measured and undressed absorption modeled reflectance of dye 720 on cotton-fabric substrate. The model is using a scatter density of 1.9.

For Dye 720, the iterative analysis demonstrated an ideal model fit with four critical features, similar to the original undressed reduced spectra. The enhanced parameters from the constrained optimization are provided in Table 3. The scatter density was optimized to a value of C_s = 1.65. The measurement-optimized critical feature parameters resulted in a significantly improved fit with the measured reflectance data, with the mean squared error improving from 0.026 to 0.00037. The measurement-optimized results are shown in Figure 4.

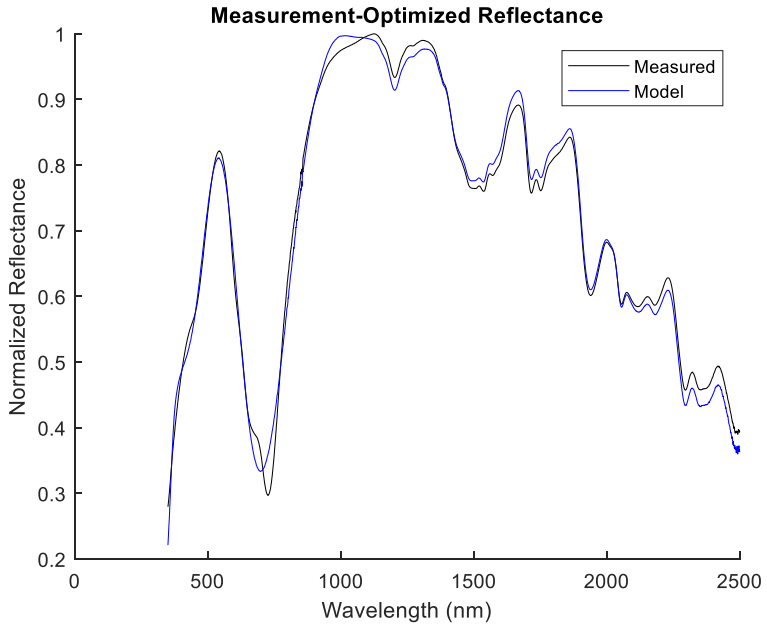

Figure 4: Comparison of measured and measurement-optimized modeled reflectance of dye 720 on cotton-fabric substrate. The model is using a scatter density of 1.65.

Table 3: KM-720 Measurement-Optimized Critical Feature Parameters

Wavelength	Peak Amplitude	Full-Width Half-Height
205	0.20	432
492	0.10	303
1179	0.62	999
805	0.32	434

The measurement-optimization, using a multi-variable gradient descent algorithm, provides model parameters that very closely align with the measurement reflectance. This approach captures the macro-spectral characteristics well; however, minor inflections are more difficult to capture due to their minimal impact on the mean squared error optimization function. This can be seen with the lack of distinction between the two inflection points near 680 nm and 720 nm. In order to correct for this, the mean squared error calculation from Eq. (14) was updated into a wavelength-weighted calculation. As a result, wavelengths over which the dye exhibits key absorption characteristics are weighted as a higher contribution within the mean squared error calculation. This update is shown in Eq. (15).

$$MSE = 0.9 \cdot \frac{1}{(\lambda_2 - \lambda_1)} \sum_{n=\lambda_1}^{\lambda_2} \left(R_n(\lambda) - R_s(\lambda)\right)^2 + \cdots$$
$$0.1 \cdot \frac{1}{(\lambda_1 - \lambda_0) + (\lambda_N - \lambda_2)} \left(\sum_{n=\lambda_0}^{\lambda_1} \left(R_n(\lambda) - R_s(\lambda)\right)^2 + \sum_{n=\lambda_2}^{N} \left(R_n(\lambda) - R_s(\lambda)\right)^2 \right) \quad (Eq. 15)$$

In the wavelength-weighted equation, λ_0 represents the measurement starting wavelength, λ_1 represents the starting wavelength for the dye's key absorption activity region, λ_2 represents the end of the dye's key absorption activity region, and λ_N represents the ending wavelength of the measurement. The dye's high activity region, between λ_1 and λ_2, contributes 90% of the optimization response for the mean squared error calculation, ensuring good alignment in this critical spectral region. Applying this adjustment to dye 720 results in significantly improved inflection point characterization, as shown in Figure 5.

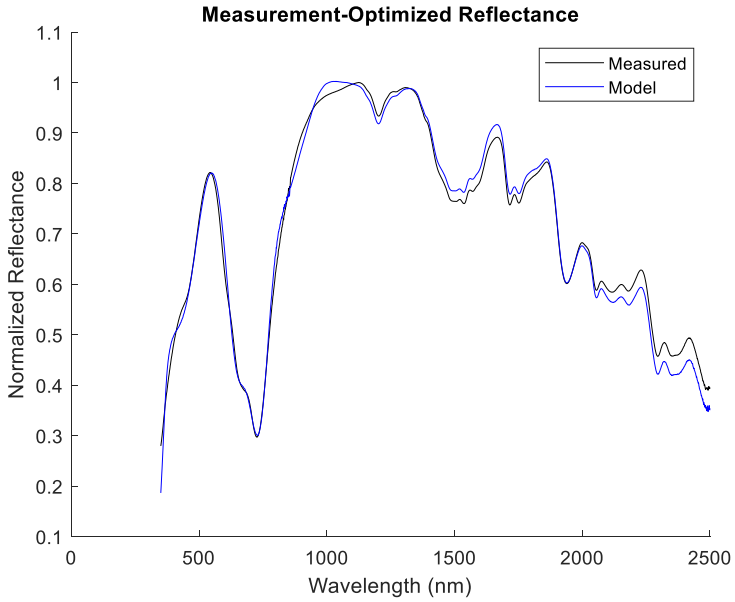

Figure 5: Comparison of the measured reflectance and the measurement-optimized wavelength-weighted modeled reflectance of dye 775 on cotton-fabric substrate. The model is using a scatter density of 1.17 and a weighted activity region spanning 650 nm-750 nm.

The critical feature parameters for the updated wavelength-weighted results are shown in Table 4. With the new optimization function, the ideal performance was found using 6 critical features. With the un-weighted optimization function, these two additional critical features were unable to provide improved characterization near the key spectral activity region.

Table 4: KM-720 Measurement-Optimized Wavelength-Weighted Critical Feature Parameters

Wavelength	Peak Amplitude	Full-Width Half-Height
255	0.569	255
493	0.478	381
668	0.139	129
765	0.356	124
867	0.676	303
1121	0.902	671

The parametric model in Table 4 provides a highly accurate characterization of the measured diffuse reflectance, which can support higher fidelity modeling capabilities.

5. Case-Study Modeling of Reflectance

The critical feature wavelength-weighted optimization steps were performed for 12 NIR-SWIR absorbing COTS dyes on a cotton-fabric substrate, and the results were compared to the undressed absorption-based models (see Figures 5-27). These results demonstrate the optimization model's capability for simulating measured diffuse reflectance, based on the reduction of absorption spectra, and using critical feature isolation and projection. This analysis continues that of [14 and 16] by construction of a parametric model using reduced basis-function representations of IR absorption spectra, and the application of a measurement-based optimization solution.

Dye KM-775

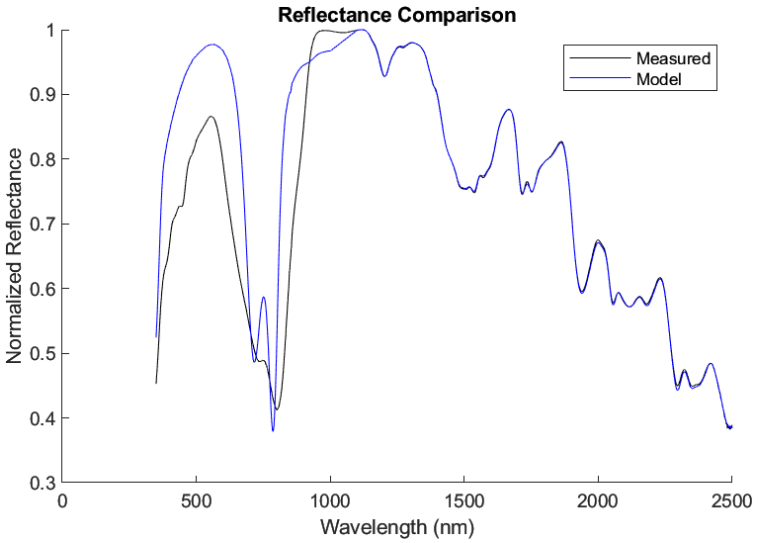

Figure 6: Comparison of measured reflectance and the undressed absorption model reflectance of dye 775 on cotton-fabric substrate. The model is using a scatter density of 1.6.

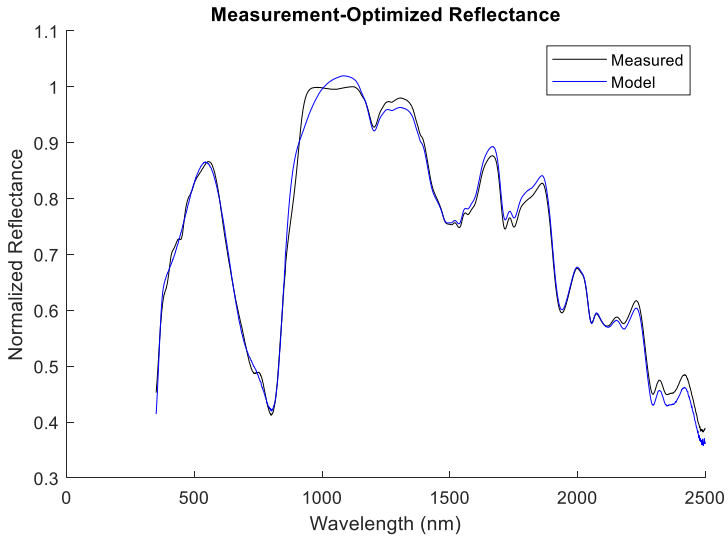

Figure 7: Comparison of the measured reflectance and the measurement-optimized wavelength-weighted modeled reflectance of dye 775 on cotton-fabric substrate. The model is using a scatter density of 1.44 and a weighted activity region spanning 450 nm-850 nm.

Table 5: KM-775 Measurement-Optimized Wavelength-Weighted Critical Peak Parameters

Wavelength	Peak Amplitude	Full-Width Half-Height
193	0.206	311
473	0.248	588
730	0.070	244
843	0.113	97
915	0.255	389
1236	0.688	983

Dye KM-778

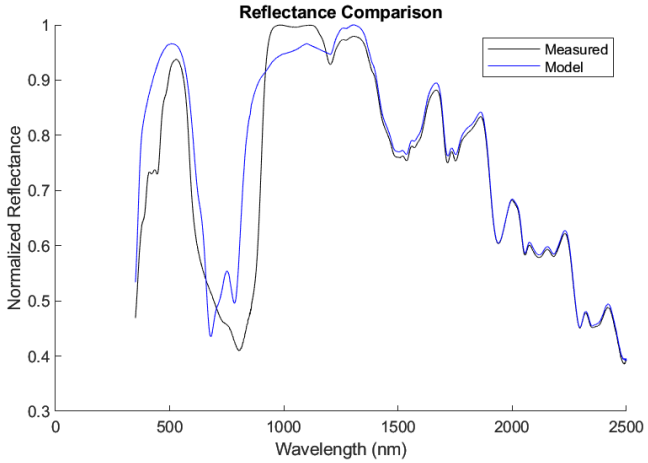

Figure 8: Comparison of measured reflectance and the undressed absorption model reflectance of dye 778 on cotton-fabric substrate. The model is using a scatter density of 1.8.

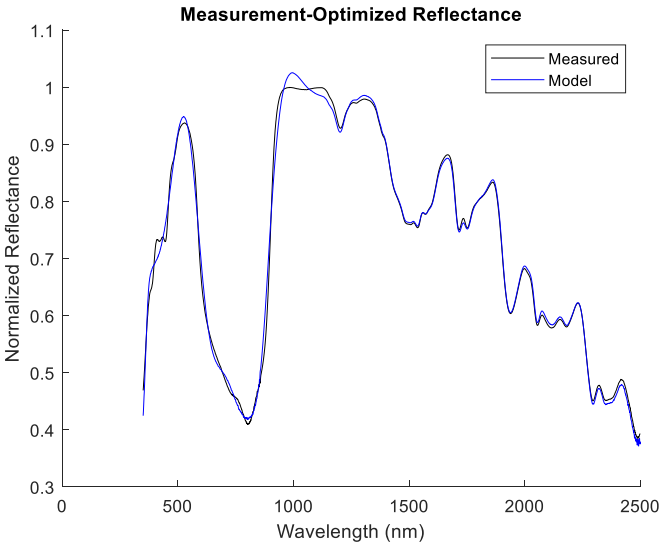

Figure 9: Comparison of the measured reflectance and the measurement-optimized wavelength-weighted modeled reflectance of dye 778 on cotton-fabric substrate. The model is using a scatter density of 0.60 and a weighted activity region spanning 350 nm-850 nm.

Table 6: KM-778 Measurement-Optimized Wavelength-Weighted Critical Peak Parameters

Wavelength	Peak Amplitude	Full-Width Half-Height
187	0.559	468
484	0.347	314
668	0.273	262
816	0.441	387
880	0.576	432
886	0.401	125
1117	0.631	480
1143	0.503	521
1364	0.720	514
1618	0.445	498

Dye KM-780

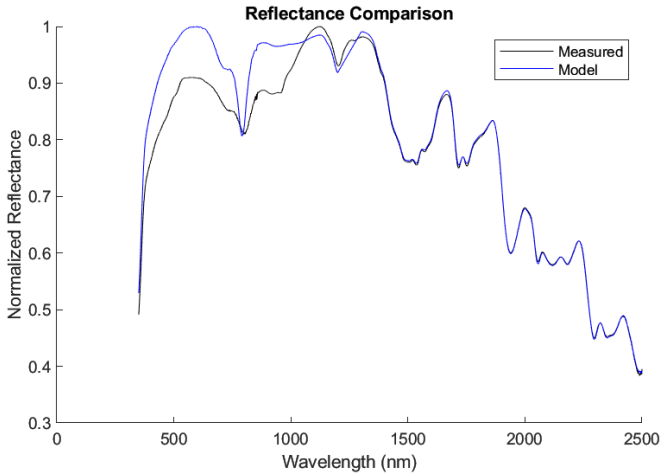

Figure 10: Comparison of measured reflectance and the undressed absorption model reflectance of dye 780 on cotton-fabric substrate. The model is using a scatter density of 0.95.

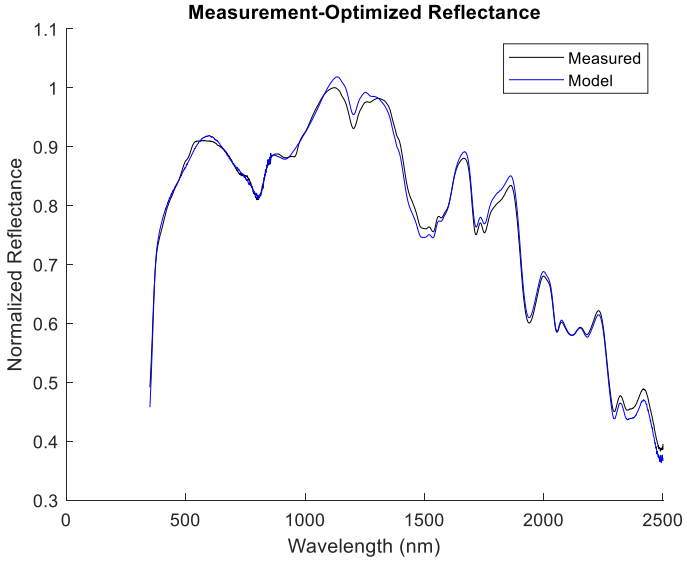

Figure 11: Comparison of the measured reflectance and the measurement-optimized wavelength-weighted modeled reflectance of dye 780 on cotton-fabric substrate. The model is using a scatter density of 0.90 and a weighted activity region spanning 650 nm-1050 nm.

Table 7: KM-780 Measurement-Optimized Wavelength-Weighted Critical Peak Parameters

Wavelength	Peak Amplitude	Full-Width Half-Height
247	0.030	604
316	0.141	584
540	0.330	557
746	0.181	386
156	0.244	355
985	0.877	568
825	0.037	67
1367	0.765	666

Dye KM-825

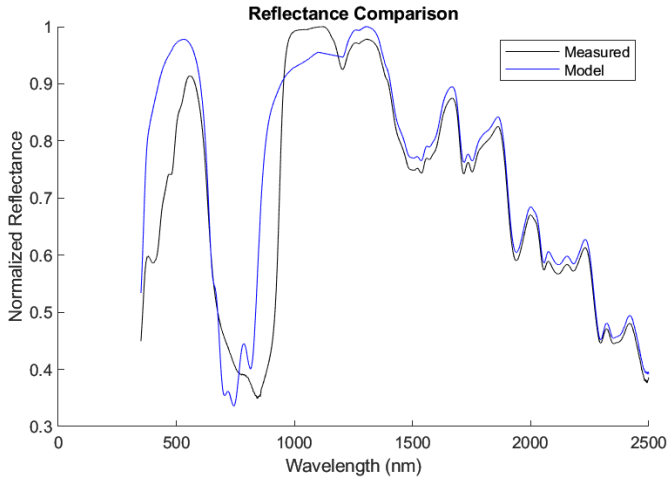

Figure 12: Comparison of measured reflectance and the undressed absorption model reflectance of dye 825 on cotton-fabric substrate. The model is using a scatter density of 1.9.

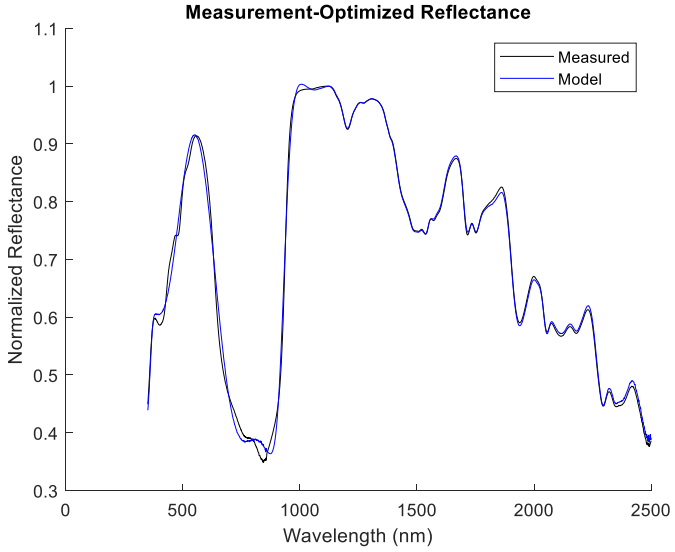

Figure 13: Comparison of the measured reflectance and the measurement-optimized wavelength-weighted modeled reflectance of dye 825 on cotton-fabric substrate. The model is using a scatter density of 0.48 and a weighted activity region spanning 350 nm-1150 nm.

Table 8: KM-825 Measurement-Optimized Wavelength-Weighted Critical Peak Parameters

Wavelength	Peak Amplitude	Full-Width Half-Height
139	0.327	584
495	0.274	400
808	0.730	547
928	0.330	101
1066	0.589	447
1267	0.701	502
1495	0.816	555
1802	0.958	807

Dye KM-832

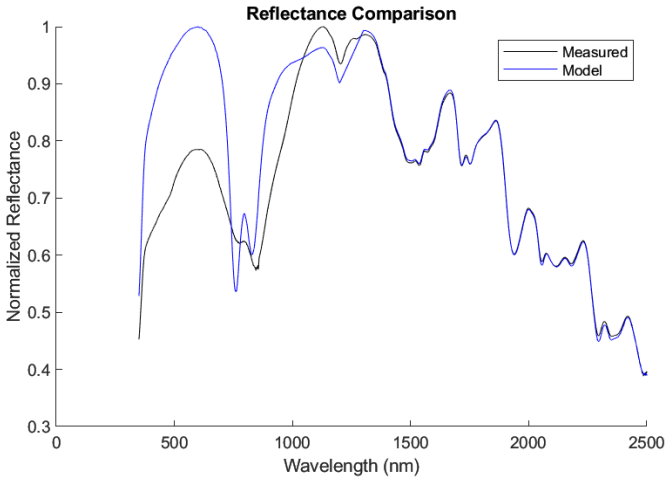

Figure 14: Comparison of measured reflectance and the undressed absorption model reflectance of dye 832 on cotton-fabric substrate. The model is using a scatter density of 1.4.

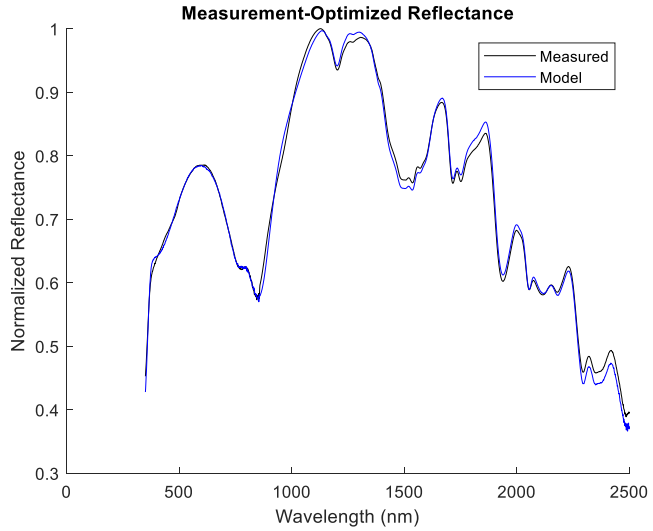

Figure 15: Comparison of the measured reflectance and the measurement-optimized wavelength-weighted modeled reflectance of dye 832 on cotton-fabric substrate. The model is using a scatter density of 0.61 and a weighted activity region spanning 650 nm-850 nm.

Table 9: KM-832 Measurement-Optimized Wavelength-Weighted Critical Peak Parameters

Wavelength	Peak Amplitude	Full-Width Half-Height
208	0.621	249
425	0.511	562
686	0.755	669
779	0.075	115
891	0.335	153
982	0.655	324
1144	0.916	570
1426	0.804	583

Dye KM-836

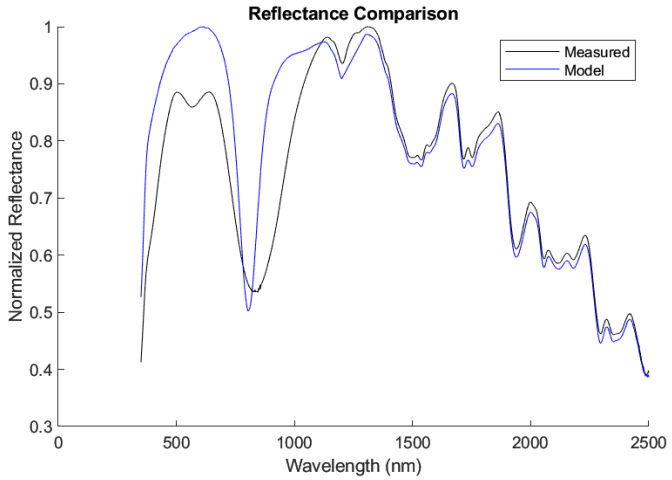

Figure 16: Comparison of measured reflectance and the undressed absorption model reflectance of dye 836 on cotton-fabric substrate. The model is using a scatter density of 1.3.

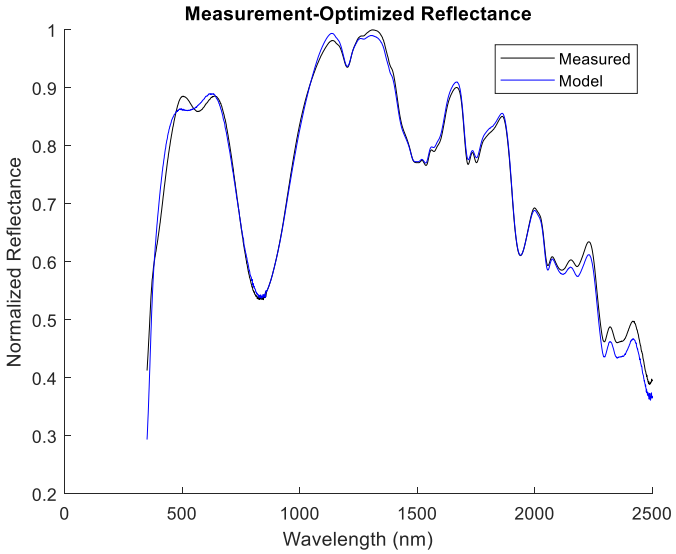

Figure 17: Comparison of the measured reflectance and the measurement-optimized wavelength-weighted modeled reflectance of dye 836 on cotton-fabric substrate. The model is using a scatter density of 1.17 and a weighted activity region spanning 450 nm-1850 nm.

Table 10: KM-836 Measurement-Optimized Wavelength-Weighted Critical Peak Parameters

Wavelength	Peak Amplitude	Full-Width Half-Height
167	0.168	996
608	0.058	332
951	0.358	445
1294	0.690	998

Dye KM-845

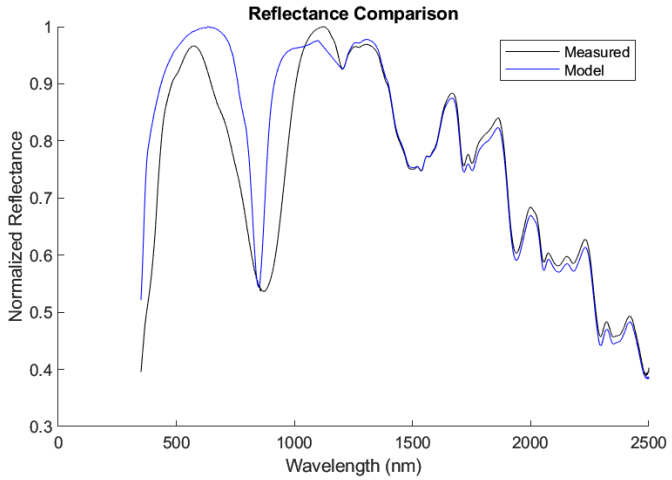

Figure 18: Comparison of measured reflectance and the undressed absorption model reflectance of dye 845 on cotton-fabric substrate. The model is using a scatter density of 1.1.

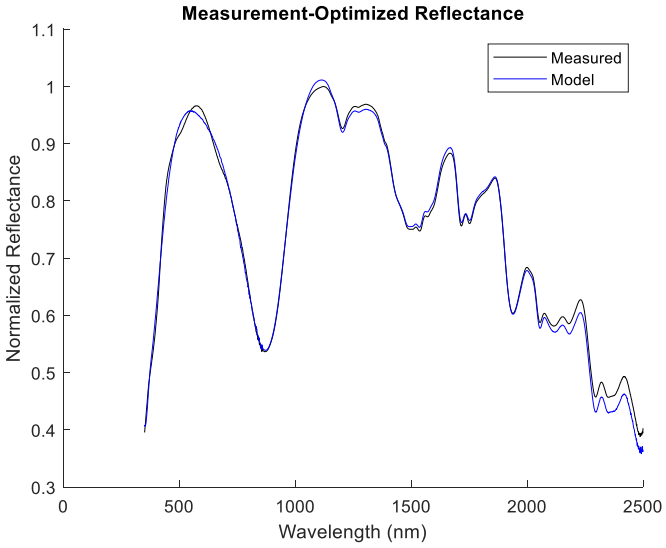

Figure 19: Comparison of the measured reflectance and the measurement-optimized wavelength-weighted modeled reflectance of dye 845 on cotton-fabric substrate. The model is using a scatter density of 1.61 and a weighted activity region spanning 450 nm-1850 nm.

Table 11: KM-845 Measurement-Optimized Wavelength-Weighted Critical Peak Parameters

Wavelength	Peak Amplitude	Full-Width Half-Height
253	0.200	619
291	0.385	11
651	0.167	702
950	0.214	247
1247	0.589	989

Dye KM-920

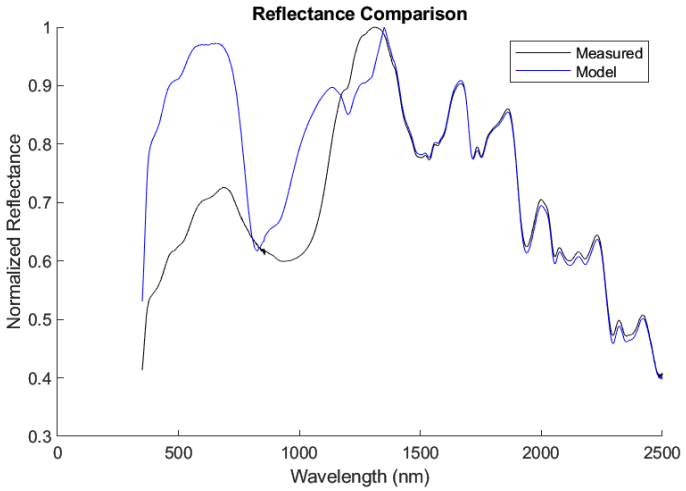

Figure 20: Comparison of measured reflectance and the undressed absorption model reflectance of dye 920 on cotton-fabric substrate. The model is using a scatter density of 1.5.

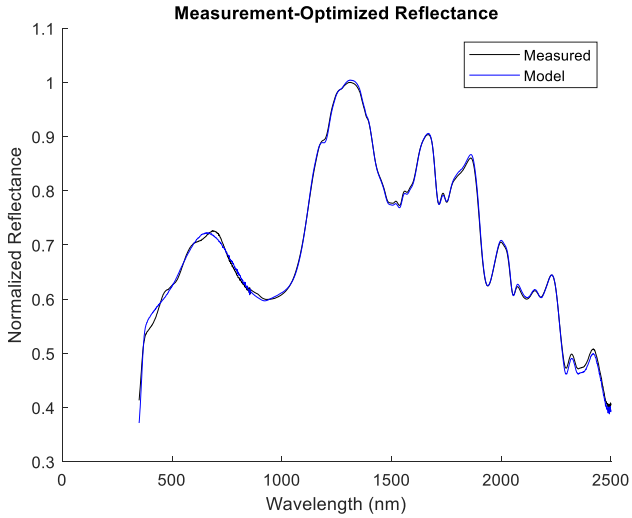

Figure 21: Comparison of the measured reflectance and the measurement-optimized wavelength-weighted modeled reflectance of dye 920 on cotton-fabric substrate. The model is using a scatter density of 1.01 and a weighted activity region spanning 450 nm-1850 nm.

Table 12: KM-920 Measurement-Optimized Wavelength-Weighted Critical Peak Parameters

Wavelength	Peak Amplitude	Full-Width Half-Height
109	0.099	651
569	0.212	830
1061	0.502	807
1119	0.116	173
1501	0.584	996

Dye KM-949

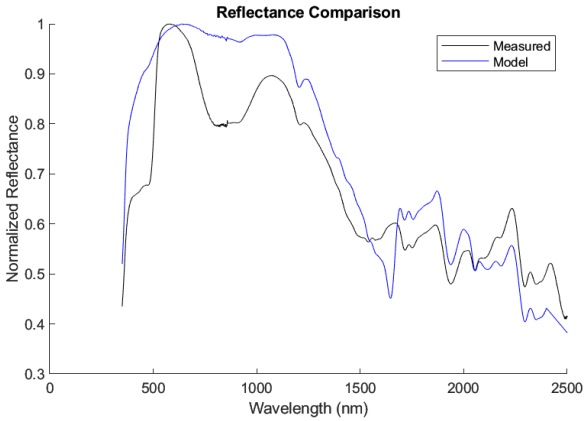

Figure 22: Comparison of measured reflectance and the undressed absorption model reflectance of dye 949 on cotton-fabric substrate. The model is using a scatter density of 1.5.

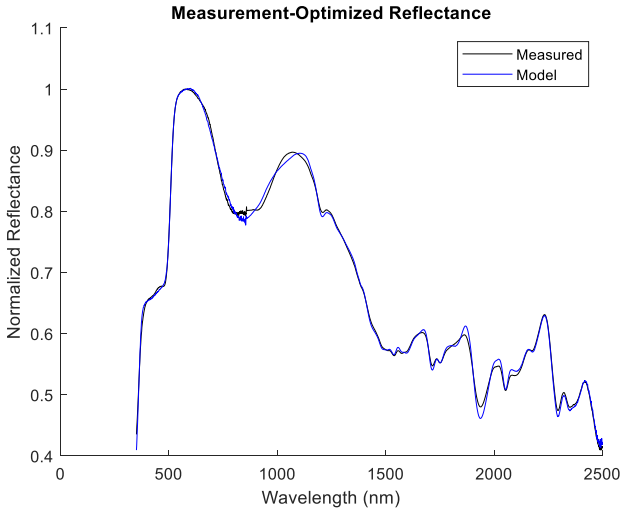

Figure 23: Comparison of the measured reflectance and the measurement-optimized wavelength-weighted modeled reflectance of dye 949 on cotton-fabric substrate. The model is using a scatter density of 0.87 and a weighted activity region spanning 450 nm-1850 nm.

Table 13: KM-949 Measurement-Optimized Wavelength-Weighted Critical Peak Parameters

Wavelength	Peak Amplitude	Full-Width Half-Height
203	0.241	301
411	0.099	462
507	0.008	49
560	0.218	643
908	0.372	695
1124	0.196	572
1421	0.598	565
1615	0.238	430
1671	0.180	165
1799	0.573	361
1841	0.126	102
1952	0.376	215

Dye KM-978

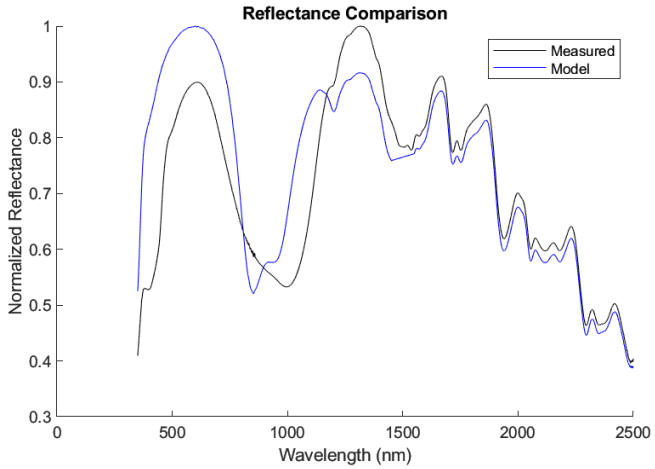

Figure 24: Comparison of measured reflectance and the undressed absorption model reflectance of dye 978 on cotton-fabric substrate. The model is using a scatter density of 1.5.

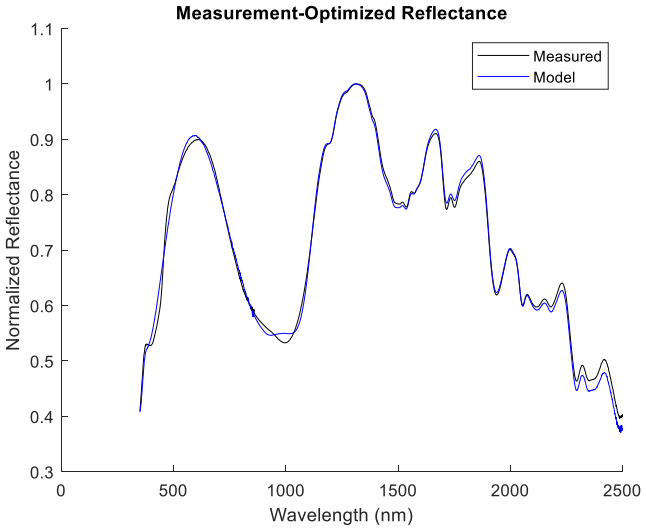

Figure 25: Comparison of the measured reflectance and the measurement-optimized wavelength-weighted modeled reflectance of dye 978 on cotton-fabric substrate. The model is using a scatter density of 0.87 and a weighted activity region spanning 450 nm-1350 nm.

Table 14: KM-978 Measurement-Optimized Wavelength-Weighted Critical Peak Parameters

Wavelength	Peak Amplitude	Full-Width Half-Height
2	0.003	338
340	0.070	565
468	0.277	808
688	0.039	929
979	0.078	307
1054	0.831	978
1106	0.344	161
1424	0.395	734

Dye KM-1072

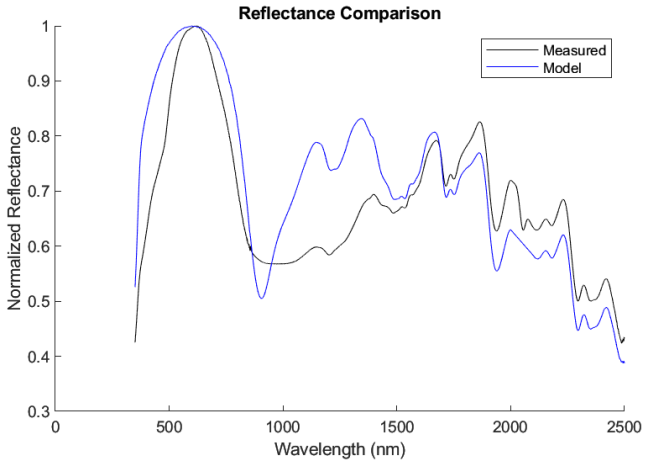

Figure 26: Comparison of measured reflectance and the undressed absorption model reflectance of dye 1072 on cotton-fabric substrate. The model is using a scatter density of 1.4.

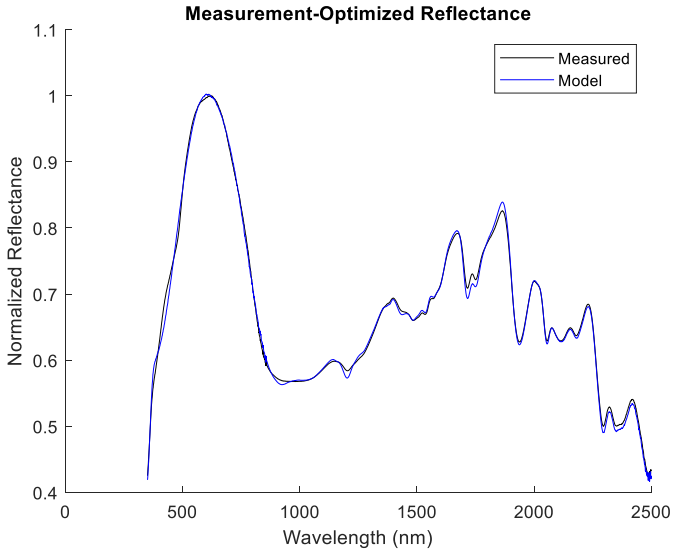

Figure 27: Comparison of the measured reflectance and the measurement-optimized wavelength-weighted modeled reflectance of dye 1072 on cotton-fabric substrate. The model is using a scatter density of 2.15 and a weighted activity region spanning 450 nm-1950 nm.

Table 15: KM-1072 Measurement-Optimized Wavelength-Weighted Critical Peak Parameters

Wavelength	Peak Amplitude	Full-Width Half-Height
109	0.032	440
150	0.037	570
483	0.097	569
689	0.060	468
923	0.130	470
1126	0.183	452
1354	0.386	406
1638	0.255	417

6. Discussion

The results from this analysis establish a proof of concept for the spectral reduction of complex measurement spectra into a significantly reduced critical feature subspace capable of maintaining the measured dielectric response characteristics for effective-medium model analysis. Optimizing the parametric model to fit the measured reflectance improved the reflectance accuracy significantly compared to the undressed parametric models based only on the absorption calculation. The optimization step was further improved by identifying each dye's prioritized wavelengths of absorption activity and applying a wavelength-weighted optimization function. As a result, these diffuse reflectance prediction models accurately capture the critical spectral elements, and can in-turn support the predictive modeling of new dye combinations and substrates.

7. Conclusion

Simulating diffuse reflectance spectra of dyed fabrics, in particular fabrics containing NIR-SWIR absorbing dyes, is important for the design of IR absorbing fabrics. This study presents and demonstrates an optimized parametric model for this purpose, which is based on the reduction of absorption spectra by means of critical feature isolation and projection. The undressed parametric model based on the absorption calculation provides the initial inputs for a multi-variable gradient descent optimization to more accurately align with the diffuse reflectance measurements. This allows the parametric model to account for measurement and processing artifacts that improve its application specificity. The reduced, optimized functions establish a modeling space that can support the mapping of functions between individual NIR-SWIR absorbing dye components and new diffuse reflectance mixtures and substrate combinations.

Acknowledgements

This project was supported by U.S. DoD programs.

References

1. C.F. Bohren and D.R. Huffman, Absorption and Scattering of Light by Small Particles, Wiley-VCH, 2004.
2. V. Dzimbeg-Malcic, Z. Barbaric-Mikocevic, K. Itric, "Kubelka-Munk Theory in Describing Optical Properties of Paper (I)," Technical Gazette 18, 1 (2011), pp.117-124.
3. P. Kubelka, F. Munk, "Ein Beitrag zur Optik der Farbanstriche," Z. Tech. Phys. (Leipzig), 12 (1931), pp. 593-601.
4. P. Kubelka, "New Contributions to the Optics of Intensely Light-Scattering Materials. Part I," J. Opt. Soc. Am., 38 (1948), pp. 448-457.
5. P. Kubelka, "New Contributions to the Optics of Intensely Light-Scattering Materials. Part II," J. Opt. Soc. Am., 44 (1954), pp. 330-335.
6. D.R. Anifimov, I.G. Golyyak, A.S. Tabalina, I.L. Fufurin, "Kramers-Kronig Relations in Spectral Analysis of Diffuse Reflected Radiation," J. Physics: Conference Series, 1348 (2019) 012084. doi:10.1088/1742-6596/1348/1/012084
7. F.W. King, "Numerical Evaluation of Truncated Kramers-Kronig Transforms," J. Opt. Soc. Am. B, Vol. 24, No. 7 (2007), pp. 1589-1595.

8. M. Bakry and L. Klinkenbusch, “Using The Kramers-Kronig Transforms To Retrieve The Conductivity From The Effective Complex Permittivity,” Adv. Radio Sci., 16 (2018), pp. 23-28.
9. K. Ohta and H. Ishida, “Comparison Among Several Numerical Integration Methods for Kramers-Kronig Transformation,” Applied Spec., Vol. 42, No. 8 (1988), pp. 952-957.
10. D. Lay, Chapter 7, Linear Algebra and Its Applications (Second Edition), Addison-Wesley, New York (2000), pp. 441-486)
11. R. Viger, S. Ramsey, T. Mayo, S.G. Lambrakos, “Parametric Modeling of Reflectance Spectra for Dyes and Their Mixtures in Fabrics Using Reference Spectra,” Journal of Electromagnetic Waves and Applications, Vol. 33, No. 9, pp. 1163-1171, (2019).
12. Fabricolor Holding International Product List, Laser and Fluorescent dyes, UV and NIR dyes, security inks and other optically functional materials, Code FHI 7206.
13. American Dye Source, Inc., ADS 775PI, CAS # 207399-07-3, 555 Morgan Boulevard, Baie D’Urfe, Quebec, Canada.
14. R. Viger, S.A. Ramsey, T. Mayo, S.G. Lambrakos, “Case-Study Estimation of Dielectric Response Functions for NIR-SWIR Absorbing Dyes by Inverse Analysis of Diffuse Reflectance,” Naval Research Laboratory Memorandum Report, Naval Research Laboratory, Washington, DC, NRL/5708/MR-2022/1, May24, 2022.
15. R. Viger, S.A. Ramsey, T. Mayo, S.G. Lambrakos, “Reduction of Absorption Spectra for NIR-SWIR Absorbing Dyes Using Critical Feature Identification and Projection,” Naval Research Laboratory Memorandum Report, Naval Research Laboratory, Washington, DC, NRL/5708/MR-2022/2, Aug4, 2022.
16. R. Viger, S.A. Ramsey, T. Mayo, S.G. Lambrakos, “Estimation of Dielectric Response Functions for NIR-SWIR Absorbing Dyes by Inverse Analysis of Diffuse Reflectance,” Journal Electromagnetic Waves and Applications, 2023.